Co-design and experimental validation of a gyroscopic stabilizer for powered two-wheelers

Giulio Panzani, Davide Todeschini, Matteo Corno, Davide Sette and Sergio M. Savaresi

***Abstract*—Roll dynamics of powered two-wheelers (PTW) are unstable at low speed and their active control could improve both safety and comfort. The paper proposes the co-design of a stabilization system based on Control Momentum Gyroscopes (CMGs) which, with their compact package and low power request, are a fascinating option in particular for PTW, where on-board energy and size constraints make the design of a proper roll torque actuator challenging. The joint design of the actuator and its control law is proposed by defining a multi-objective optimization problem, which also turns into a tool that allows the designer to steer the parameters choice in different directions. The resulting prototype is manufactured, installed on a motorcycle, tested and experimentally validated in several conditions.**

***Index Terms*—Powered two-wheelers control, gyroscopic stabilization, mechatronic co-design, multiple-objective optimization design**

I. Introduction

CONTROL momentum gyroscopes (CMGs) are a well-known torque actuator technology which is successfully employed for the stabilization and control of the angular dynamics of various systems, making use of the gyroscopic principle. Compared to reaction wheels (RWs), which feature a simpler mechanical design and easier operation, CMGs offer the significant advantage of delivering higher torque for a given actuator power [1]. This makes CMGs ideal for space applications (where power thriftiness is of paramount importance) and maritime ones (where large torques are requested).

When considering ground vehicles, CMGs do not show the same success. The main reason is the predominantly 2-dimensional – planar – motion of such vehicles, where the use of a gyroscopic stabilizer finds little room. Even when considering the 3-dimensional roll and pitch dynamics of a car, semi-active or active suspensions are generally preferred. Conversely, two-wheeled vehicles could benefit from gyroscopic stabilization: in fact, their 3D motion shows a strong coupling between the lateral and roll dynamics, highly dependent on the vehicle speed.

Within the context of Advanced Driver Assistance Systems (ADAS) for powered two-vehicles (PTW) [2], the capability of stabilizing the vehicle roll dynamics could be efficiently exploited, for instance, to implement an automated emergency braking system that require a complete vehicle stop in response to rider sickness or faint. Beside the dynamics related issues, two-wheelers feature the additional challenge of managing the trade off between space limitations and power requirement. Given these premises, the gyroscopic actuation technology seems very promising for powered two-wheelers as they can yield a roll torque to control the vehicle dynamics, at a low power cost.

The available scientific literature on PTW gyroscopic stabilization shows the potential of this technology, but it is far from being complete, as also remarked in [3, 4]. Some papers use gyroscopic stabilization to showcase specific features of some control strategies: [5, 6, 7, 8, 9] propose various interpretations of linearised state feedback control; similarly, [10, 11] explore robust control using $\mathcal{H}_\infty$ and $\mathcal{H}_2$ methods. Veering toward non linear control, one should consider [12], where a piecewise affine control is tested in simulation on a simplified vehicle dynamic model, and [13, 14, 15] which propose Fuzzy and Adaptive Sliding Mode control. Other papers make use of gyroscopic stabilization in combination with non standard vehicle configurations: for example the autonomous bike discussed in the simulation study [16] has no steering capability and makes use of the gyroscope to change direction. Similarly, an MPC approach is used in [17] to stabilize a simulated bicycle where the steer angle is considered fixed. Finally [18, 19] consider also active steering and achieve both stabilization and path tracking.

In the literature, the preferred stabilization approach is to use only the roll angle measurement as feedback. This choice does not take full advantage of the commonly available Inertial Measurement Units capable of providing, beside the estimate of the roll angle, also direct measures of the roll rate; moreover it disregards the fact that the flywheels might experience an undesired drift. This drift is a consequence of errors in the roll angle estimation or vehicle unbalances, that cause the real equilibrium position to differ from the zero roll value one. Within this perspective, the presence of a rider on the vehicle makes the stabilization problem even more challenging as their non constant posture can be seen as a time-varying system perturbation. The only work that considers riders is [20] where, however, the control strategy aims at inducing stable periodic roll oscillations, for medical purposes. As one can see, the available experimental validations of gyroscopic stabilizers are only partially satisfactory, since they do not consider the rider presence, and make use of unnecessarily restricting assumptions.

Furthermore the open scientific literature does not deal with the the design and the sizing of the gyroscopic actuator itself. In most case the actuator is given *a priori* and is a starting

G. Panzani, D. Todeschini, M. Corno and S.M. Savaresi are with Dipartimento di Elettronica, Informazione e Bioingegneria, Politecnico di Milano, Italy. Corresponding author: giulio.panzani@polimi.it

D. Sette is with Ducati Motor Holding s.p.a, Borgo Panigale, Italy

This work has been supported by the European project ADAS&ME under grant agreement No 688900.

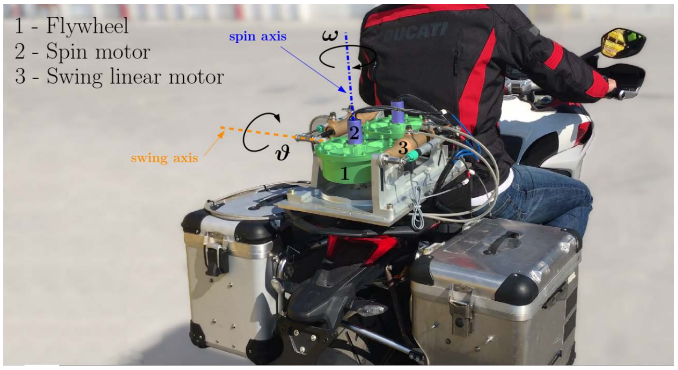

Fig. 1. The gyroscopic actuator employed in this work with its two counter-rotating gyros, mounted on the test vehicle.

point to design a control law. The only work on the gyroscopic actuator design applied to PTWs is [3] where numerical and simulation analyses address the following aspects: different stabilizer architectures, the role of active or passive stabilizer and a systematic study of its effect on the vehicle motion and handling.

This paper contributes to the highlighted missing points. In particular, it focuses on the gyroscopic stabilization of a PTW at low/null speed, proposing an integrated *co-design* approach which jointly addresses the actuator and the control parameters design, taking into direct consideration the size, power and control constraints typical of PTW. The overall procedure, firstly discussed by means of simulations, is experimentally validated on a motorcycle showing how the designed actuator and the controller achieve stabilization in a realistic scenario where sensor bias and riders-induced unbalances are natively present.

In Section II, the overall system is introduced, discussing the actuator architecture, the modelling and the resulting cascaded controller structure. Section III addresses the mechatronic project as an optimization problem whose outcome is both the actuator and the control system parameters. The stabilizing controller details are discussed in Section IV, ranging from the selected control structure, the available degrees of freedom and their role in achieving a robust performance with respect to sensing errors and parameter uncertainties. Section V concludes the paper with the experimental validation of the designed actuator and controller, using a ridden motorcycle.

II. System description

A. System overview

This work considers a standard touring motorcycle. Based also on the considerations outlined in [3], the actuator architecture features a couple of counter-spinning and counter-swinging gyroscopes (see Fig. 1 and Fig. 3). The two spinning axes are aligned with respect to the vehicle vertical axis and are independently driven by two electric motors (element 2, marked in blue). Two hydraulic linear actuators (element 3, orange coloured) move each flywheel (enclosed in the green shell, element 1) around the swing axis, normally aligned with the vehicle pitch one. The choice of such configuration is to be preferred to other options, as the counter-movement of the gyroscopes yields a null parasitic torque on the vehicle. In addition, the actuator generates a torque along the vehicle roll axis only if the swing axis are actively actuated, see [3].

B. Modelling

The overall system dynamics are described by the set of equations (1). For their derivation, the interested reader can refer to [5].

$$Mlg\sin\rho - I\ddot{\rho} = \sum_{i=1}^{2} I_{g_z}\omega_i\dot{\vartheta}_i\cos\vartheta_i \tag{1a}$$

$$I_{g_x}\ddot{\vartheta}_i - I_{g_z}\dot{\rho}\omega_i\cos\vartheta_i + F_{d,\vartheta_i} = \tau_{\vartheta_i} \tag{1b}$$

$$I_{g_z}\dot{\omega}_i + I_{g_z}\ddot{\rho}\sin\vartheta_i + I_{g_z}\dot{\rho}\dot{\vartheta}_i\cos\vartheta_i + F_{d,\omega_i} = \tau_{\omega_i} \tag{1c}$$

Equation (1a) pertains the motorcycle dynamics which – at low vehicle speed – can be described as an inverted pendulum. The left side collects the destabilizing gravitational torque and the roll inertia; the right side models the roll gyroscopic torque, proportional to the flywheel spinning inertia I_{g_z} and the product between the spinning (ω_i) and the swinging ($\dot{\vartheta}_i$) velocities. The suffix $i = 1, 2$ refers to the corresponding flywheel and has been added to keep the notation compact.

Equations (1b) and (1c) describe, respectively, the swing and spin rotation dynamics and both equation hold for each of the two flywheel. The control inputs τ_{ϑ_i}, τ_{ω_i} appear on the right hand side, causing respectively the swing and spin accelerations $\ddot{\vartheta}_i$ and $\dot{\omega}_i$. All the other terms can be regarded as disturbances: some are related to the spin and swing coupling due to the gyroscopic effect and the others describe the system non-idealities, lumped in the terms F_{d,ϑ_i} and F_{d,ω_i}. As an example, F_{d,ω_i} contains all the friction torques that must be compensated to reach the spinning speed ω_i.

In equation (1a), the vehicle, the rider and the flywheels are lumped into a single set of parameters: M is the overall mass, located at the equivalent distance from the ground l, and I is equivalent roll inertia. These parameters are computed considering the vehicle ($m_v = 260$ kg), the rider ($m_d = 70$ kg) and the flywheels as three point-like masses set at a certain height ($l_v = 0.6$ m, $l_d = 0.9$ m and $l_g = 0.8$ m) from the ground. While the vehicle parameters are known, the same doesn't hold for the rider's weight which is a constant, though uncertain, parameter. Moreover, the model considers a rider that is rigidly connected to the motorcycle; in reality, riders are free to shift their weight on the saddle [21]. Since it is practically impossible to accurately model how any rider would actively behave, it is better to consider a simplified model and test the controller against the rider's movement. The flywheel mass m_g and the spinning inertia I_{gz} are the result of the design procedure, proposed in Section III.

It is worth mentioning that, when deriving equations (1), some features of the considered application allow for some simplifications. The roll equivalent inertia I neglects the flywheels rotational inertia contributions, as they are orders of magnitude smaller than the vehicle ones. In equation (1a) and (1b) the gyroscopic effect has been simplified keeping only the terms $\omega_i\dot{\vartheta}_i\cos\vartheta_i$ and $I_{g_z}\dot{\rho}\omega_i\cos\vartheta_i$ which are outstanding with respect to others, due to the very high value of ω_i.

C. Control architecture

A cascade control architecture is well suited for the system described in (1), where the stabilizing roll torque depends on the spinning rate and the swinging one. As shown in Fig. 2, two inner independent controllers – enclosed in the darker shade – are used, one for each axes angular speed. The outer control loop – in the brighter shade – computes the reference angular velocities, eventually yielding the desired stabilizing roll torque.

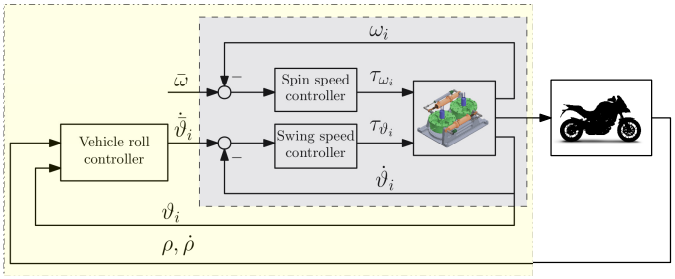

Fig. 2. Block diagram of the cascade control scheme.

The gyroscopic torque model, see (1a), suggests that the swing angle ϑ_i should be kept as small as possible, in order to avoid the end-stops and to maximize gyroscopic efficacy. To do so, the term $I_{g_z}\omega_i$ is maximized: on one side the mechanic flywheels design tries to increase as possible their spin inertia I_{g_z}; on the other side, the spinning speed controller is designed so to track high reference values (thousands of rpms). Both objectives in practice yield a low-bandwidth spin controller that aims to track a constant reference, as the amount of torque τ_{ω_i} needed to dynamically change the values of ω_i would result in an oversized spin motor. For this reason, the spin speed reference is a constant design parameter. The flywheel spin thus acts like a roll gyroscopic torque booster and the torque dynamic modulation is delegated to the swing speed controller, designed to track a reference speed with a sufficiently high bandwidth.

III. Actuator mechatronic design

A. Problem definition

A multi-objective optimization for the design of the CMG actuator parameters is proposed. The PTWs gyroscopic stabilization calls for a mechanical and control co-design. In fact, in PTWs (and in general narrow-track vehicles), weight, space and power limitations are tight; as a result the actuators parameters are typically not simply constrained within a range of admissible values, but should be optimized. On the other side, the control goal, *i.e.* the vehicle upright stabilization, is highly dependent on the actuator design: the consequence of a wrong actuator sizing is not a suboptimal control performance but the impossibility of stabilizing the vehicle. Thus, a mechanical-and-control joint design is required.

The optimal choice of plant (physical quantities) and control parameters (*e.g.* control law gains, control variable trajectories, etc..) can be addressed as an optimization problem within different frameworks, see [22, 23]. In this work the so called *simultaneous* co-design formulation is employed, where the values of the physical (x_p) and control (x_c) variables are found by solving an optimization problem where a cost function $J(x_p, x_c)$ embeds both plant and control objectives. Some remarks on the proposed approach follow.

In linear plant and feedback control law co-design problems it is very efficient to express control objectives analytically, see for instance [24]. Analytic formulations are usually not available when nonlinear co-design is addressed. A common practice is to define a reference scenario and to evaluate the control performances in a simulation-based manner. Moreover, no particular assumptions are made on the control structure and the direct optimization of the control variables trajectories is done [25]. This kind of approach, at a later stage, requires the control system specialist to find a suitable control law that mimics the optimized control. Despite the apparent complexity this approach is common in literature – see [23, 26] – as it leaves the control specialist the necessary degrees of freedom in the design of the closed-loop control law that, for nonlinear systems, is not a standard problem. The proposed CMGs co-design follows this approach, avoiding the explicit definition of a feedback control law, which is addressed at a later stage in Section IV.

Another distinctive feature of the proposed co-design is the use of the inverse system dynamics. In the hypothesis that the flywheels are perfectly counter swinging and spinning at the same constant speed, the nonlinear equation (1a) can be rewritten

$$\dot{\vartheta} = \frac{1}{\cos\vartheta} \cdot \left(\frac{1}{2I_{g_z}\omega} \left(Mlg \sin\rho(t) - I\ddot{\rho}(t) \right) \right)$$

and analytically integrated, yielding the time trajectory of the swing angle:

$$\vartheta(t) = \arcsin\left(\frac{1}{2I_{g_z}\omega} \int_0^t \left(Mlg \sin\rho(t) - I\ddot{\rho}(t) \right) dt \right). \quad (2)$$

Thanks to equation (2), closed-loop roll angle trajectories can be imposed and the corresponding swing angle trajectory computed. The control input τ_ϑ can be finally found by means of equation (1b). This simplifies the optimization problem, as the system dynamics no longer appear in the constraints.

The actuator co-design is hence addressed by solving the following problem:

$$\begin{aligned} \min_{x_p, x_c} \quad & J(x_p, x_c) \\ \text{s. t.} \quad & f(x_p, x_c) \leq 0 \end{aligned} \quad (3)$$

where the cost function $J(x_p, x_c)$ and the constraints $f(x_p, x_c) \leq 0$ are evaluated on the following reference scenario. We consider the stabilization of the vehicle starting from a non equilibrium condition $\rho_0 \neq 0, \dot{\rho}_0 = 0$. In such manoeuvre, though simplified, the initial roll value ρ_0 summarizes the non-idealities and disturbances that the controller should cope with. We consider $\rho_0 = 2^\circ$ which is the resulting COG inclination when the driver bends out from the vehicle vertical axis of about 30°, a rather extreme situation.

The elements of the co-design problem (3) are detailed in the following.

1) Decision variables x: these are the parameters that characterize the actuator, both in terms of physical (x_p) and control (x_c) parameters. They are:

$$x = [x_p \,|\, x_c] = [R \quad \alpha \quad h \quad \bar{\omega} \,|\, \Omega_\rho \quad \xi_\rho]\,. \tag{4}$$

The first three parameters define the flywheel geometry, hence the resulting spin, swing inertia (I_{g_z} and I_{g_x}) and mass m_g. Having opted for a hollow cylinder – whose symmetrical shape helps to avoid vibrations induced by unbalanced loads – the external radius R, the cylinder height h and the ratio between the internal r and the external radius $\alpha \in [0, 1]$ completely define the flywheel geometry, see also Figure 3. The spin speed

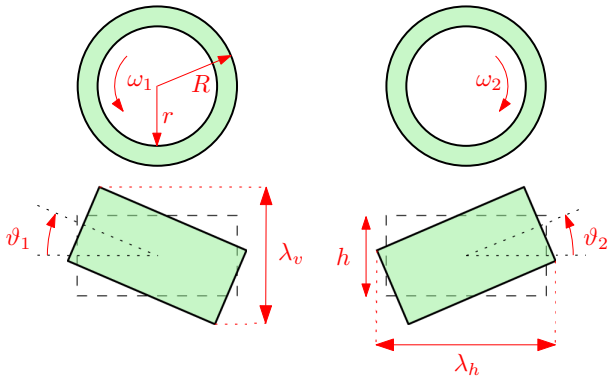

Fig. 3. Schematic representation of the flywheels.

reference $\bar{\omega}$ – tracked by the dedicated spin controller – plays a role both from a physical and a control point of view: on one side a high spinning speed concerns the designer in terms of power consumption and mechanical flywheel stresses but, on the other, allows for a higher available roll torque.

The last two design parameters are control related ones. They parametrize the time-domain evolution of the vehicle roll angle, during the uprise manoeuvre. Such trajectory matches the one of a second order dynamic system (as suggested by the roll equation (1a)) and can be generally described with the following expression:

$$\rho(t) = \frac{\rho_0}{\sqrt{1-\xi_\rho^2}} e^{-\xi_\rho \Omega_\rho t} \cos\left(\Omega_\rho \sqrt{1-\xi_\rho^2} \cdot t\right). \tag{5}$$

For a given roll angle evolution, the required swing angle trajectory is given by (2). Thus, thanks to the inverse dynamics, closed-loop performance become actual decision variables rather than control objectives. Decoupling the closed-loop behaviour from the control law that practically yields it allows for better interpretability of the optimization results and for a wider flexibility in the design of the control law, which can also address secondary objectives that are not originally included in the actuator design in order to keep the optimization problem simple.

2) Cost function: there are several competing objectives that the design should take into consideration and for this reason the co-design is in fact a Multi-Objective Optimization (MOO) problem. In this paper we opted to approach the MOO using the *scalarization* method, by means of a weighted sum $J(x)$ of five different cost functions $J_i(x)$:

$$J(x) = \sum_{i=1}^{5} w_i J_i(x). \tag{6}$$

The use of *scalarization* rather than *Pareto methods*, see [27], is common in co-design optimization-based problem, as it provides a unique solution and allows the designer to incorporate preferences or objective rankings with relative simplicity. Moreover, the high number of objectives included in the optimization makes the use of *Pareto methods* difficult, as the resulting Pareto front is no longer easily representable.

Straightforward plant design objectives are the overall actuator mass ($J_1(x)$) and its bulk ($J_2(x)$). For the defined flywheel shape, the mass is:

$$J_1(x) = m_g = \pi \varrho h R^2 \left(1 - \alpha^2\right) \tag{7}$$

where ϱ is the density of the material. The space occupied by the actuator depends not only its geometric dimensions, but also on the swing flywheel movement during the manoeuvre. The maximum horizontal (λ_h) an vertical (λ_v) occupied spaces (see also Figure 3) are:

$$\begin{aligned} \lambda_h &= \max_t \left(2R\cos\vartheta(t) + h\sin\vartheta(t)\right) \\ \lambda_v &= \max_t \left(2R\sin\vartheta(t) + h\cos\vartheta(t)\right) \end{aligned}. \tag{8}$$

where $\vartheta(t)$ is the flywheel swing angle during the motorcycle rise, computed thanks to (2). A synthetic bulk cost function is thus defined:

$$J_2(x) = \lambda = \sqrt{\lambda_h^2 + \lambda_v^2}. \tag{9}$$

The costs $J_3(x)$ and $J_4(x)$ account for energetic considerations. The former considers the kinetic energy stored in each flywheel

$$J_3(x) = E_{spin} = \frac{1}{2} I_{g_z} \bar{\omega}^2. \tag{10}$$

The latter describes the maximum actuation power during the manoeuvre:

$$J_4(x) = P_{sw} = \max_t \tau_\vartheta(t)\dot{\vartheta}(t) \tag{11}$$

where $\dot{\vartheta}(t)$ is computed as in (2) and $\tau_\vartheta(t)$ from the swing dynamics in equation (1b), neglecting the non idealities lumped in the term F_{d,ϑ_i}.

Finally, $J_5(x)$, is equal to the value of the flywheel swing angle at the end of the rising manoeuvre

$$J_5(x) = \vartheta_\infty. \tag{12}$$

This cost quantifies the control-oriented goal of keeping the flywheels close to the zero swing angle position. This indirectly accounts for the end-stops presence, not explicitly modelled in the system dynamics. More importantly, one should recall that the gyroscopic roll torque decreases with the swing angle and becomes zero when $\vartheta = 90°$, nullifying the actuator effectiveness. This issue can be mitigated with a proper design of the outer controller, but it is still important to include this parameter in the cost function.

In weighted-sum MOO weights selection is a known crucial point [28]. Weights w_i usually accomplish two tasks: they normalize the different cost functions and reflect system designer preferences among the different objectives. Traditional techniques normalize each cost by dividing for a reference value, typically related to the maximum or minimum cost function value within the admissible range of the optimization variables [28]. In co-design MOO, compared to more classic decision making MOO, design variables boundaries are usually loose or difficult to be defined a-priori: for instance, one can think of the minimum flywheel size, or the range of the control design variables which are both difficult to be strictly defined. For this reasons, a systematic normalization approach is not viable as the reference cost function values would reflect unrealistic situations, ill-posing the co-design problem. Thus, we opted to compute the weights as the reciprocal of a limit acceptable value (according to the *designer*) of the cost function value J_i^*, thus $w_i = 1/J_i^*$. In this way the weights embed the designer preferences and also normalize each the cost function. Notice that a very similar approach is used in [29]. The reference cost function values, along with the corresponding weights, are reported in Table I.

3) Constraints: the co-design constraints are

$$0 \leq R \leq R_{\max} \quad (13a) \qquad 0 < \Omega_\rho \leq \Omega_{\rho,\max} \quad (13e)$$
$$0 \leq \alpha < 1 \quad (13b) \qquad 0 < \xi_\rho \leq 1 \quad (13f)$$
$$0 \leq h \leq h_{\max} \quad (13c) \qquad \mathrm{Im}\left(\vartheta(t)\right) = 0. \quad (13g)$$
$$0 \leq \bar{\omega} \leq \bar{\omega}_{\max} \quad (13d)$$

Constraints (13a)-(13e) keep the design parameters within their significance range. The last two constraints are the most interesting ones. Equation (13f) imposes the asymptotic stability of the roll dynamics, as makes the roll angle converging to zero. Constraint (13g) enforces the feasibility of the rising manoeuvre. For a given roll trajectory, defined by Ω_ρ and ξ_ρ, but there is no guarantee that the actuator can provide the required roll torque, that depends on the swing angle trajectory ϑ(t): preventing imaginary solutions of (2) certifies the admissibility of design.

The existence of a solution for the co-design problem depends only on the constraint (13g), that is satisfied whenever the $\arcsin$ argument in equation (2) is sufficiently small. This can be always achieved with high values of the spin speed $\bar{\omega}$ or flywheel inertia I_{g_z}: relaxing the upper bounds in equations (13a), (13c) and (13d) can thus help, whenever optimization infeasibility becomes an issue.

TABLE I
COST FUNCTIONS ACCEPTABLE LIMITS AND CORRESPONDING WEIGHTS FOR THE DEFINITION OF (6)

J_i^*	m_g^*	λ^*	E_{spin}^*	P_{sw}^*	ϑ_∞^*
value	10 Kg	0.20 m	$2 \cdot 10^4$ J	5 W	1.25 rad
w_i	0.1	5	$5 \cdot 10^{-5}$	0.2	0.8

B. Results and analysis

The optimization problem (3) that minimizes (6) over the variables (4) enforcing the constraints (13) is solved in Matlab using the *fmincon* routine. Table II lists the optimal parameters and the corresponding cost function terms.

TABLE II
OPTIMAL DESIGN PARAMETERS.

Optimization variable	**value**
R	8 cm
α	0.71
h	4.2 cm
$\bar{\omega}$	9800 rpm
Ω_ρ	0.65 Hz
ξ_ρ	0.68

Cost function	**value**
$J_1 = m_g$	3.2 kg
$J_2 = \lambda$	0.22 m
$J_3 = E_{spin}$	8100 J
$J_4 = P_{sw}$	2.4 W
$J_5 = \vartheta_\infty$	35°

A sensitivity analysis complements these results. Fig. 4 shows the outcomes of the optimization whend carried out for different values of the weights. In each column, the i^{th} weight is changed (for example, in the first column the weight $\bar{m}_g$, referred to the cost function J_1): the top row shows the effect of such change on the optimal design variables whereas the bottom one depicts the impact on the cost function terms J_i. For the sake of a more clear representation, instead of parametrizing the different lines according to the weights values, the corresponding cost function changes are used.

For instance, the first column shows how the optimal actuator design changes if a reduction of the overall flywheel mass is needed. The top plot reveals that reducing the mass (lines where $m_g < 0\%$) leads to a geometric redistribution in the flywheels that result less thick (the parameter h is reduced) and radially fuller (α increases). However, such redistribution is non-optimal in terms of gyroscopic inertia since some mass is moved from a peripheral to a central position and the spin speed $\bar{\omega}$ needs to increase. It is interesting to notice that all the design objectives are equivalently competing: in fact, for each cost modification an almost equivalent change is experienced in all the other cost functions. Thus, subgrouping of competing objectives is not feasible and remarks the challenges in the application of Pareto approaches for the solution of the MOO problem.

Beside the tradeoffs, the sensitivity analysis provides quantitative indications for the designer. As an example, inspecting the third column, if one wants to almost half the spin reference speed, they have to cope with at least a 15% increase of volume (λ), flywheel mass, swing angle and swing actuation power. These numbers are useful to assess if such spin speed reduction is compatible with other design constraints and feasibility.

As final remark, notice how the closed-loop parameters ξ_ρ and Ω_ρ are mostly sensitive to the swing related variables, namely the swing actuation power P_{sw} and the final swing angle ϑ_∞: the roll stabilization closed-loop response can be fastened (thanks to the increase of Ω_ρ) almost linearly *w.r.t.* the available swing actuation power and decreasing the damping of the complex poles ξ_ρ has a significant impact on the reduction of the swing angle ϑ_∞.

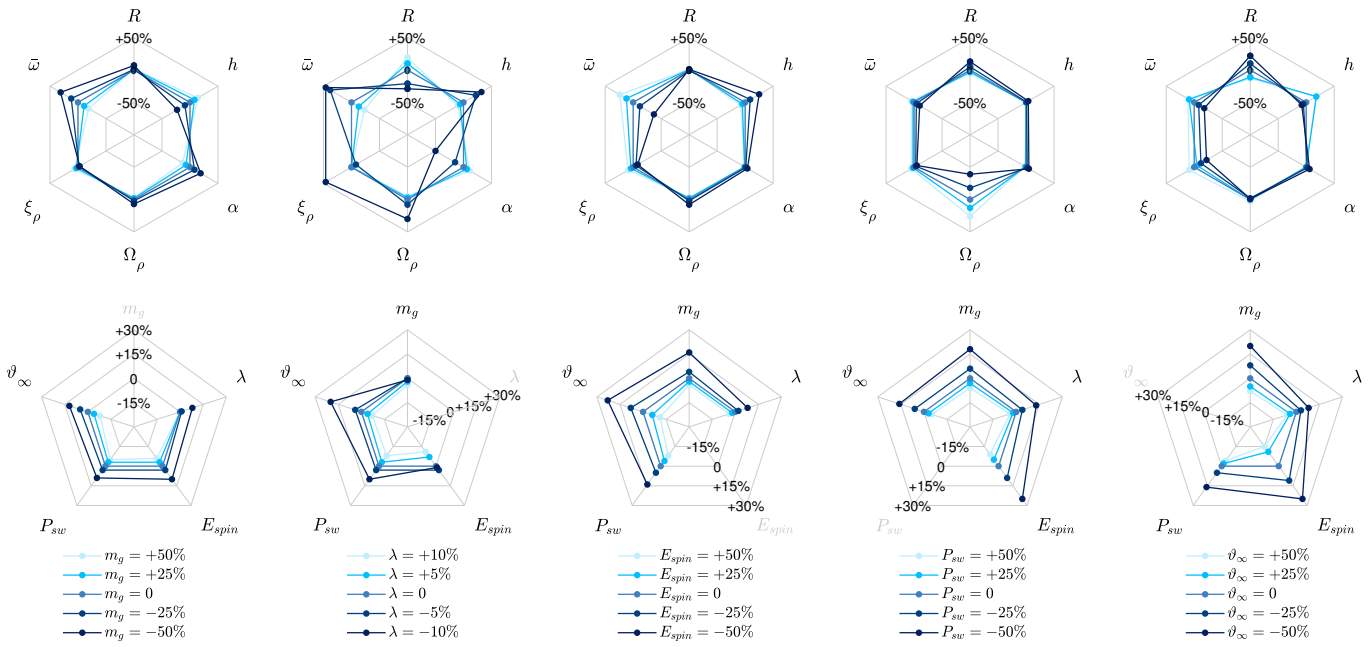

Fig. 4. Sensitivity analysis of the design parameters and corresponding cost function with respect to the weights w_i values.

IV. Controller design

A. Internal controllers - Spin and swing speed

The inner, as in Fig. 2, controllers are classical servo-loops closed on the swing and spin dynamics. They are designed considering two factors. Firstly, the spin speed controller must be capable of reaching and keeping the target speed $\bar{\omega}$. The second requirement is control-oriented: the optimal design sets quantitative targets for the closed-loop roll dynamics, *i.e* the natural frequency Ω_ρ and the damping ξ_ρ, and the internal swing speed loop must be faster than these dynamics to effectively apply the cascade control architecture. In practice, considering that the required dynamics feature a settling time of $t_{set} = 1.8s$ an internal swing control bandwidth higher than 4Hz should be guaranteed for the swing speed controller. These considerations lead to a simplified model of the swing and spin (14) dynamics.

$$\dot{\vartheta}_i = \dot{\bar{\vartheta}}_i, \qquad \dot{\omega}_i = 0. \tag{14}$$

B. External controller - Roll dynamics

After the system co-design is solved, the system control specialist must design a control law which is capable of stabilizing the vehicle in a general condition, not only in the considered reference scenario. This, unfortunately, is usually not an immediate task, see [25]. However, the proposed co-design sets clear targets for the external controller: the roll closed-loop dynamics must match a second order asymptotically stable system with parameters Ω_ρ and ξ_ρ. This naturally suggests the use of a linear state-feedback control law, whose parameters are computed by means of the pole placement method. Within this framework, it is also possible to address other closed-loop objectives, important for a practical controller realization, but secondary with respect to the main vehicle stabilization goal. These secondary objectives can be achieved without any modification to the actuator design: for this reason they have not been explicitly included in the co-design, in order to keep the optimization problem as simple as possible.

To address the control law design, a control-oriented model of the system is needed. Firstly, the roll dynamics equations (1a) are rewritten as

$$\ddot{\rho} = \frac{Mlg}{I}\rho - \frac{I_{g_z}}{I}\bar{\omega}\left(\dot{\bar{\vartheta}}_1 + \dot{\bar{\vartheta}}_2\right) \tag{15a}$$

$$\begin{aligned}\dot{\vartheta}_1 &= \dot{\bar{\vartheta}}_1 \\ \dot{\vartheta}_2 &= \dot{\bar{\vartheta}}_2,\end{aligned} \tag{15b}$$

where (15a) comes from the linearisation of the dynamics around the nominal stabilized equilibrium, $\rho, \dot{\rho} = 0$ and $\vartheta_{1,2} = 0$ and constant speed $\bar{\omega}$. Equations (15b) reflect the control-oriented description of the swing dynamics, as in (14).

A more convenient form of the control-oriented model is obtained by considering the *counter* (16a) and *in-phase* (16b) swing movements of the flywheels:

$$\begin{aligned}\vartheta &= \frac{\vartheta_1 + \vartheta_2}{2} \\ \dot{\vartheta} &= \frac{\dot{\vartheta}_1 + \dot{\vartheta}_2}{2}\end{aligned} \tag{16a}$$

$$\begin{aligned}\Delta\vartheta &= \frac{\vartheta_1 - \vartheta_2}{2} \\ \Delta\dot{\vartheta} &= \frac{\dot{\vartheta}_1 - \dot{\vartheta}_2}{2}\end{aligned} \tag{16b}$$

The linearised system equations (15) can be then written in the state-space form:

$$\dot{\mathbf{x}} = \left[\begin{array}{ccc|c} 0 & 1 & 0 & 0 \\ \mathtt{a} & 0 & 0 & 0 \\ 0 & 0 & 0 & 0 \\ \hline 0 & 0 & 0 & 0 \end{array}\right] \mathbf{x} + \left[\begin{array}{c|c} 0 & 0 \\ \mathtt{b} & 0 \\ 1 & 0 \\ \hline 0 & 1 \end{array}\right] \mathbf{u} \tag{17}$$

with $\mathtt{a} = \frac{Mlg}{I}$, $\mathtt{b} = -2\frac{I_{g_z}}{I}\,\bar{\omega}$ and

$$\mathbf{x} = \left[\begin{array}{c} x_1 \\ x_2 \\ x_3 \\ \hline x_4 \end{array}\right] = \left[\begin{array}{c} \rho \\ \dot{\rho} \\ \vartheta \\ \hline \Delta\vartheta \end{array}\right] = \left[\begin{array}{c} \mathbf{x}_\vartheta \\ \hline \mathbf{x}_\Delta \end{array}\right] \quad \mathbf{u} = \left[\begin{array}{c} u_\vartheta \\ u_\Delta \end{array}\right] \left[\begin{array}{c} \dot{\vartheta} \\ \Delta\dot{\vartheta} \end{array}\right]$$

Equations (17) reveal that the roll and the *counter-phase* swing dynamics ϑ are decoupled form the *in-phase* $\Delta\vartheta$ ones; thus the *in-phase* dynamics $\mathbf{x}_\Delta$ control is addressed at a later stage.

The closed-loop roll and *counter-phase* system dynamics ($\mathbf{x}_\vartheta$) are further manipulated, based on the following considerations:

- the state vector $\mathbf{x}_\vartheta$ is augmented including the integral of the swing angle ϑ

$$\mathbf{x}_\vartheta = \left[\begin{array}{cccc} \rho & \dot{\rho} & \vartheta & \vartheta_\int \end{array}\right]^T$$

- a state feedback control law is implemented, including a bias term β corrupting the roll angle measure.

$$u_\vartheta = \mathbf{K^T y} = \left[\begin{array}{cccc} k_{\dot{\rho}} & k_\rho & k_\vartheta & k_{\vartheta_\int} \end{array}\right] \left[\begin{array}{c} \rho + \beta \\ \dot{\rho} \\ \vartheta \\ \vartheta_\int \end{array}\right]$$

  This additional variable models the roll angle estimation uncertainties and the lateral vehicle unbalances (due to asymmetric loads or driver posture) that imply a non null roll angle equilibrium position.

The closed-loop dynamics eventually become:

$$\dot{\mathbf{x}}_\vartheta = \left[\begin{array}{cccc} 0 & 1 & 0 & 0 \\ (\mathtt{a} + \mathtt{b}k_{\dot{\rho}}) & \mathtt{b}k_\rho & \mathtt{b}k_\vartheta & \mathtt{b}k_{\vartheta_\int} \\ k_{\dot{\rho}} & k_\rho & k_\vartheta & k_{\vartheta_\int} \\ 0 & 0 & 1 & 0 \end{array}\right] \mathbf{x}_\vartheta + \left[\begin{array}{c} 0 \\ \mathtt{b}k_{\dot{\rho}} \\ k_{\dot{\rho}} \\ 0 \end{array}\right] \beta \tag{18}$$

Equations (18) reveal that the control of the roll dynamics, matching the parameters Ω_ρ and ξ_ρ, could be achieved with the sole feedback of the roll and the roll rate measures (*i.e.* setting $k_\vartheta = k_{\vartheta_\int} = 0$). However, in presence of a non-zero roll bias β (that could be caused by a movement of the rider, for example), the swing angle, which features a marginally stable dynamics, would diverge. To avoid this issue, one could set a non-null reference roll angle, compensating for the bias. However, finding this value is not trivial and practically infeasible as the compensation would need to be extremely precise.

The hereby solution is to include the swing angle in the feedback variables ($k_\vartheta \neq 0$) to stabilize its dynamics: in case of roll biases, the flywheel divergence is prevented and this indirectly yields the vehicle robust stabilization. Moreover, including the swing integral variable in the feedback retrieves the angle back towards the desirable null position. The idea of activating a swing angle lure strategy at the end of the stabilization manoeuvre, has been presented in [15]. We implement such idea in a more formal and practical way, that does not require any *end-of-stabilization* trigger (that indeed makes the approach in [15] quite difficult to be applied in practice).

The benefits of including the flywheel variables ϑ and $\vartheta_\int$ in the feedback are shown in Fig. 5, that shows the vertical stabilization when the roll measure is corrupted with bias, with the three considered feedback alternatives. The upper plot shows the measured roll angle – affected by the bias β – and the lower plot the flywheel swing angle. When

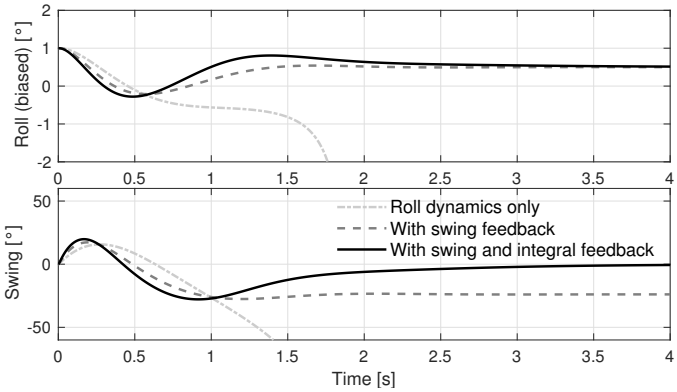

Fig. 5. Simulation of an uprise stabilization with a biased roll angle measure using different choices of feedback variables.

only the roll variables are used for the feedback action the system is stabilized only for few seconds and, as the flywheel angle reaches high values, the gyroscopic effect is no longer enough to produce the torque required to keep the vehicle in the non-equilibrium position. The inclusion of the swing variables allows the effective stabilization of the vehicle, and when the swing integral is included the flywheels relocation to the centered position is obtained. As expected, the controller stabilizes the vehicle around a non-zero roll angle (in particular around the roll value that matches the bias β).

The definition of the controller parameters $\mathbf{K}$, relies on the pole placement method. The two additional degrees of freedom reflect in an augmented vector of desired closed-loop poles:

$$\lambda_{des} = \left[\begin{array}{c} -\xi_\rho\Omega_\rho \pm j\Omega_\rho\sqrt{1-\xi_\rho^2} \\ \lambda_\vartheta \\ \lambda_{\vartheta_\int} \end{array}\right].$$

The position of the two additional poles is chosen according to the following rationale:

1) the two poles must be located at a sufficient low frequency with respect to the internal actuator controller ones, to preserve the cascaded controller architecture;
2) the smaller pole location defines the settling time of the flywheels in the centered position;
3) higher values of λ_ϑ and $\lambda_{\vartheta_\int}$ yield a smaller sensitivity of the flywheel swing angle to the bias affecting the measure;
4) increasing the values of λ_ϑ and $\lambda_{\vartheta_\int}$ requires an increase of actuator power (as in (11));
5) the choice of λ_ϑ and $\lambda_{\vartheta_\int}$ has an impact on the system robustness *w.r.t.* the driver mass value.

Fig. 6 graphically represents points 3) and 4). To quantitatively assess point 5), Fig. 7 shows the couples λ_ϑ - $\lambda_{\vartheta_\int}$ which result in a successful vehicle stabilization (gray area) for different driver mass, m_d, values. As the driver mass increases the feasibility region shrinks. Still, this happens for significant variations (over 30 kilograms with respect to the nominal

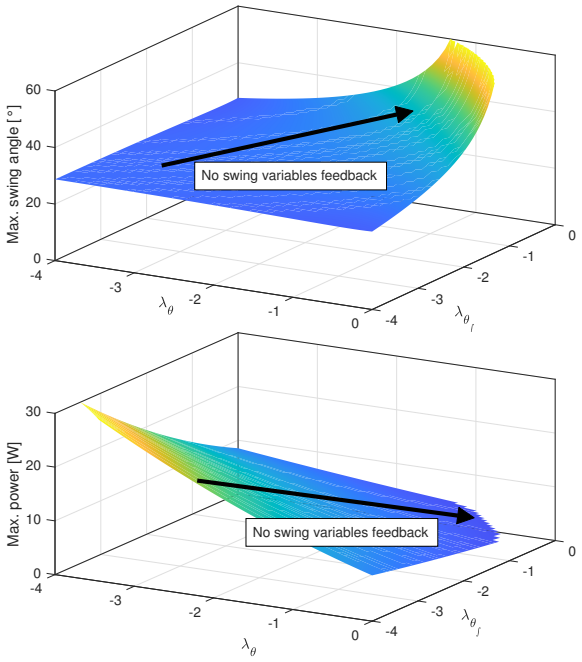

Fig. 6. Effect of different locations of the desired closed-loop poles λ_ϑ and λ_{ϑ_f} on the maximum swing angle and actuator power in a roll biased vertical stabilization manoeuvre.

value); in view of a possible real application of the gyroscopic stabilizer one could make use of available tools for mass estimation, see *e.g.* [30] and adapt the controller parameters accordingly.

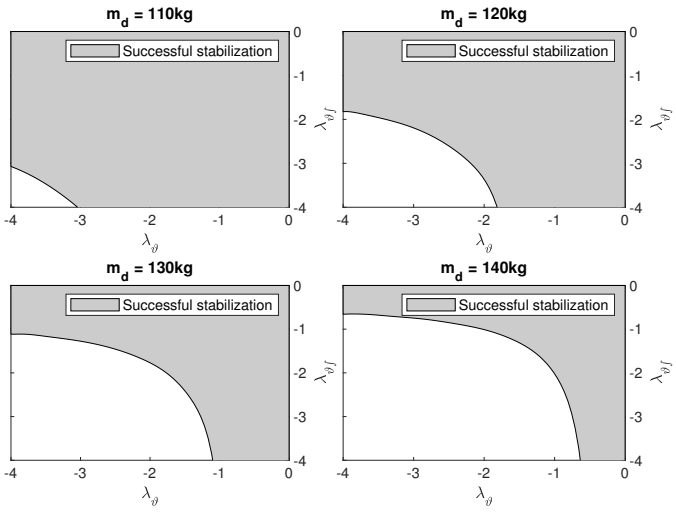

Fig. 7. Combinations of λ_ϑ - λ_{ϑ_f} values that result in a successful vehicle stabilization starting from a 1° initial condition (grey area) as function of the driver mass (70kg is the nominal controller design value).

The stabilization of the *in-phase* dynamics can follow the same rationale used for the *counter-phase* ones, acting on the control variable $u_\Delta = \Delta\dot{\vartheta}$. Using the state-feedback control law $u_\Delta = k_\Delta \mathbf{x}_\Delta$ the closed-loop dynamics become:

$$\dot{\mathbf{x}}_\Delta = k_\Delta \mathbf{x}_\Delta. \tag{19}$$

The asymptotic stabilization of the *in-phase* dynamics is much simpler, being independent from the vehicle roll dynamics. The value of k_Δ is related to the location of the closed-loop pole of such dynamics: since *in-phase* movements are expected to be related to small flywheel differences – for example in terms of mass, frictions etc. – it is not mandatory to enforce fast closed-loop dynamics.

V. Experimental results

The previous sections focused on designing the system and the controller. The design has been carried out under some simplifying hypothesis. This section, by building and testing a prototype – according to the results of the optimization based design – provides proof that the simplifying assumptions do not limit the applicability of the proposed approach. The design of Section III lead to the actuator shown in Fig. 1: the prototype is installed in place of the tail box of a Ducati Multistrada 1260, whereas the saddlebags house the hydraulic and the electronic components. The flywheel weighs $4\,\mathrm{kg}$ and their yaw inertia is $0.0169\,\mathrm{kg{\cdot}m^2}$. The slightly different flywheels parameters, with respect to the nominal design, are due to a 8mm disk that fills the hollow cylinder, which is required to guarantee the structural integrity of the actuator and ease the spin motor anchoring. The vehicle is equipped with wheel encoders that measure the vehicle speed v, and an Inertial Measurement Unit that provides the roll rate $\dot{\rho}$ and an estimate of the vehicle roll angle ρ. The gyroscopic actuator comes with two spin motor encoders (measuring $\omega_{1,2}$), and two linear potentiometers that provide the swing angles $\vartheta_{1,2}$ and their angular rates $\dot{\vartheta}_{1,2}$.

The flywheels are set at $10\,000$ rpm. Fig. 8 shows that the spin controller tracks the reference precisely, despite the swing and roll vehicle movements occurring during the stabilization test (the one presented in the later Fig. 12). The swing speed controller features a bandwidth of approximately $7\,\mathrm{Hz}$, as visible in the reference step response shown in the bottom plot of Fig. 8. Note how the controllers successfully decouple

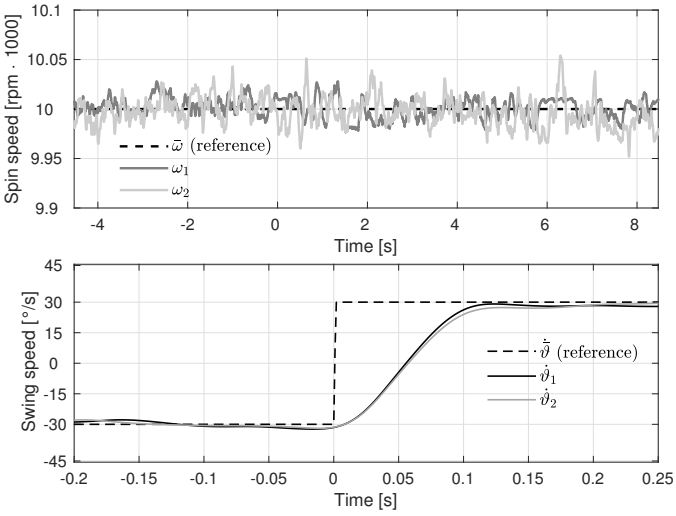

Fig. 8. Experimental spin (top) and swing (bottom) speed internal controller performance.

the spin and swing dynamics.

The location of the additional closed-loop swing poles has been tuned experimentally following the indications provided in Section IV.

Fig. 9 assesses the stabilizing capability in the co-design reference scenario (*i.e.* starting from a non zero roll angle). The vehicle roll is stabilized and the flywheel angles go back to the zero starting position. Note that the equilibrium position does not coincide with a null vehicle roll angle, as discussed. The experimental upright stabilization manoeuvre has the same settling time as the simulated one of Figure 5; one could note a slightly larger overshoot which is explained by the simplified simulation model.

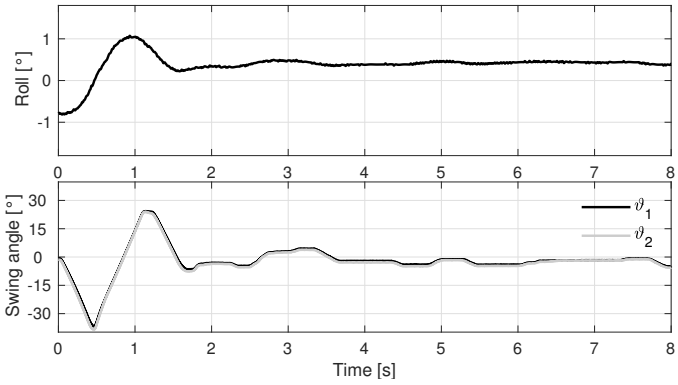

Fig. 9. Experimental vehicle upright stabilization manoeuvre.

Fig. 10 exemplifies the role of the swing angle feedback. It compares the full state (roll and swing variables) and the partial (roll variables) feedback solutions, where in the latter case the roll measure is manually compensated so to result in an almost zero value at the equilibrium. The experiments prove

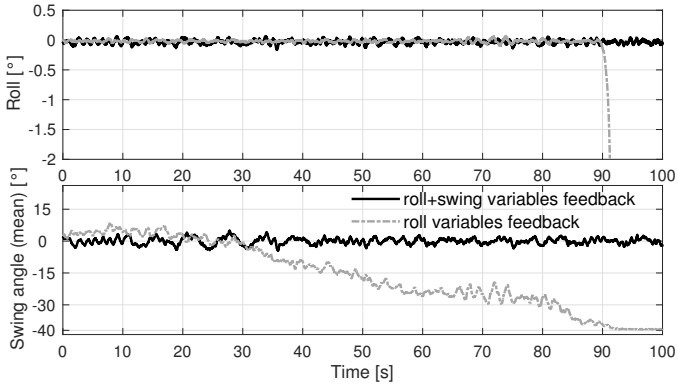

Fig. 10. Experimental comparison between the partial (roll variables) and full (roll and swing variables) state feedback.

how both controllers succeed in maintaining the motorbike upright. However, the non perfect roll reference computation causes the drift of the flywheels for *roll variables* strategy, which eventually hit the endstops and cause the motorcycle to fall.

Fig. 11 refers to an upright stabilization, with one flywheel starting from a position very close to the endstop. This experiment highlights the role of the *in-phase* controller. The *counter-phase* and *in-phase* controllers work simultaneously to stabilize the vehicle, compensate the roll angle estimate offset, eventually leading both flywheels to the zero rest position

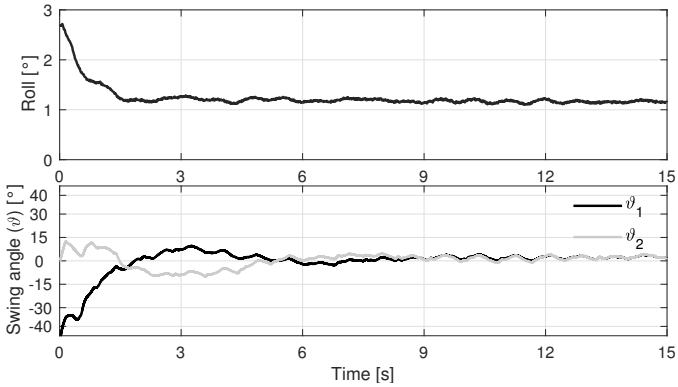

Fig. 11. Experimental vehicle upright stabilization manoeuvre with a misaligned initial flywheel angles.

The model used in the design, assumes a rigid rider; in order to check the impact of this hypothesis, we consider both external disturbances – Fig. 12 – and riders' mass and movements – Fig. 13. In the first figure, the system is initially stable and, at the vertical lines, perturbed by an external action: the roll variation immediately triggers the flywheels movement, maintaining the vehicle equilibrium. The second

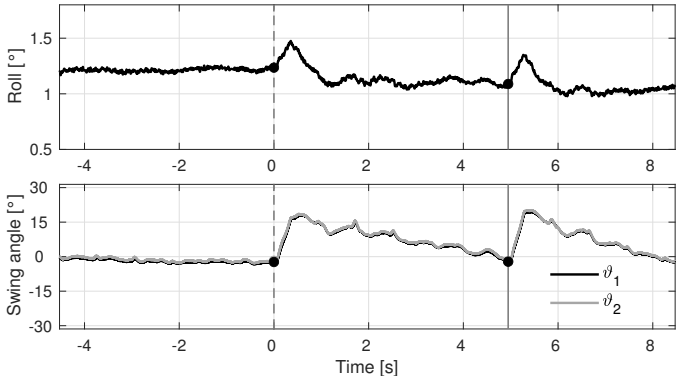

Fig. 12. Experimental assessment of the controller robustness with respect to external disturbance: at vertical lines a shove on the vehicle handlebar is applied.

figure tests three different conditions: without the rider, with the rider standing as still as possible and with the rider behaving naturally. Note that the system stability is always achieved and that the equilibrium roll reaches different values, indicating that the presence of the rider causes a lateral shift of the COG. Further, the system successfully manages time-varying unbalances induced by the rider. These unbalances result in more variable roll and swing angle trajectories that are however stable. This analysis proved the robustness of the design against rider's un-modelled behaviours.

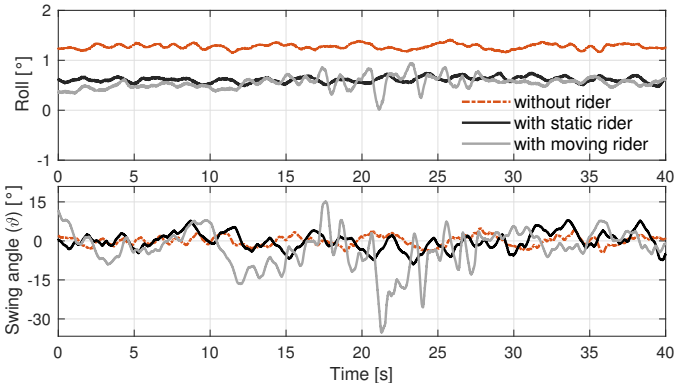

Fig. 13. Controller robustness with respect to different load conditions: without rider, with an immobile rider and with a moving rider.

VI. Conclusion

This paper tackles the vertical stabilization of powered two-wheelers (PWTs) by means of Control Moment Gyroscope (CMG). The novelty of the paper lies in the fact that not only the stabilizing control strategy is addressed, but also the design of the gyroscopic actuator. This last point is particularly relevant when outlooking a real use of such devices in the development, for instance of PWT-oriented ADAS, and it is not properly addressed in literature. In fact, the space and weight constraints typical of PWTs make the actuator design challenging. The overall co-design process is eventually validated, showing the experimental stabilization of a real vehicle.

The design of the CMG is framed within a genuine co-design approach, where the solution of a multi-objective optimization problem jointly provides both the main physical and control system parameters. The proposed cost function ensembles different objectives, by means of a weighted sum; this allows the designer to manage the relevance of each cost term according to their needs. The paper exemplifies this approach with a sensitivity analysis the uncovers the quantitative link between the physical and the control parameters.

The control strategy is based on a full state feedback. The inclusion of the swing angle and its integral provides closed-loop robustness *w.r.t.* practical issues like biases in the roll angle measure and driver movements on the saddle. The final experimental validation shows that the joint actuator and controller design succeeds in stabilizing a touring motorcycle in realistic scenarios, using a relatively compact CMG. Such results give an interesting outlook for the future employment of CMGs in powered two-wheeler applications.

References

[1] R. Votel and D. Sinclair, "Comparison of control moment gyros and reaction wheels for small earth-observing satellites," *AIAA/USU Conference on Small Satellites*, 2012.

[2] M. Corno, G. Panzani, and S. M. Savaresi, "Single-track vehicle dynamics control: State of the art and perspective," *IEEE/ASME Transactions on Mechatronics*, vol. 20, no. 4, pp. 1521–1532, 2015.

[3] R. Lot and J. Fleming, "Gyroscopic stabilisers for powered two-wheeled vehicles," *Vehicle System Dynamics*, vol. 57, no. 9, pp. 1381–1406, 2019.

[4] D. Karnopp, "Tilt control for gyro-stabilized two-wheeled vehicles," *Vehicle System Dynamics*, vol. 37, no. 2, pp. 145–156, 2002.

[5] S. C. Spry and A. R. Girard, "Gyroscopic stabilisation of unstable vehicles: configurations, dynamics, and control," *Vehicle System Dynamics*, vol. 46, no. sup1, pp. 247–260, 2008.

[6] M. Różewicz and A. Piłat, "Study on controller embedding stage using model-based-design for a bike with cmg," in *International Conference on Methods Models in Automation Robotics*, 2018, pp. 680–685.

[7] ——, "Modelling of bike steered by cmg," in *International Conference on Methods and Models in Automation and Robotics*, 2016, pp. 595–600.

[8] S.-H. Park and S.-Y. Yi, "Active balancing control for unmanned bicycle using scissored-pair control moment gyroscope," *International Journal of Control, Automation and Systems*, vol. 18, no. 1, pp. 217–224, 2020.

[9] T. Sohaimi, S. Ouchi, N. Kodani, H. Hirata, K. Takahashi, and M. Mubin, "Self-sustaining drive control of bike by gyro actuator," in *France-Japan/ 8th Europe-Asia Congress on Mecatronics*, 2014, pp. 291–296.

[10] U. Wasiwitono, A. Wahjudi, A. Saputra, and Yohanes, "Stabilization and disturbance attenuation control of the gyroscopic inverted pendulum," *JVC/Journal of Vibration and Control*, 2020.

[11] B. T. Thanh and M. Parnichkun, "Balancing control of bicyrobo by particle swarm optimization-based structure-specified mixed $h2/h\infty$ control," *International Journal of Advanced Robotic Systems*, vol. 5, no. 4, p. 39, 2008.

[12] S. Suntharasantic and M. Wongsaisuwan, "Piecewise affine model and control of bicycle by gyroscopic stabilization," in *Electrical Engineering/Electronics, Computer, Telecommunications and Information Technology Association of Thailand-Conference*, 2011, pp. 549–552.

[13] M.-H. Hsieh, Y.-T. Chen, C.-H. Chi, and J.-J. Chou, "Fuzzy sliding mode control of a riderless bicycle with a gyroscopic balancer," in *IEEE International Symposium on Robotic and Sensors Environments*, 2014, pp. 13–18.

[14] C.-H. Chi and J.-J. Chou, "Riderless bicycle with gyroscopic balancer controlled by fsmc and afsmc," in *International Congress on Ultra Modern Telecommunications and Control Systems and Workshops*. IEEE, 2015, pp. 150–157.

[15] H. Yetkin, S. Kalouche, M. Vernier, G. Colvin, K. Redmill, and U. Ozguner, "Gyroscopic stabilization of an unmanned bicycle," in *American Control Conference*, 2014, pp. 4549–4554.

[16] H. Yetkin and U. Ozguner, "Stabilizing control of an autonomous bicycle," in *Asian Control Conference*, 2013, pp. 1–6.

[17] T.-D. Chu and C.-K. Chen, "Design and implementation of model predictive control for a gyroscopic inverted pendulum," *Applied sciences*, vol. 7, no. 12, p. 1272, 2017.

[18] P. Wang, J. Yi, T. Liu, and Y. Zhang, "Trajectory tracking and balance control of an autonomous bikebot," in *IEEE International Conference on Robotics and Automation*, 2017, pp. 2414–2419.

[19] A. Beznos, A. Formal'Sky, E. Gurfinkel, D. Jicharev, A. Lensky, K. Savitsky, and L. Tchesalin, "Control of autonomous motion of two-wheel bicycle with gyroscopic stabilisation," in *IEEE International Conference on Robotics and Automation*, vol. 3, 1998, pp. 2670–2675.

[20] Y. Zhang, P. Wang, J. Yi, D. Song, and T. Liu, "Stationary balance control of a bikebot," in *IEEE International Conference on Robotics and Automation*, 2014, pp. 6706–6711.

[21] A. Doria and M. Tognazzo, "The influence of the dynamic response of the rider's body on the open-loop stability of a bicycle," *Proceedings of the Institution of Mechanical Engineers, Part C: Journal of Mechanical Engineering Science*, vol. 228, no. 17, pp. 3116–3132, 2014.

[22] H. K. Fathy, J. A. Reyer, P. Y. Papalambros, and A. Ulsov, "On the coupling between the plant and controller optimization problems," in *Proceedings of the 2001 American Control Conference.(Cat. No. 01CH37148)*, vol. 3. IEEE, 2001, pp. 1864–1869.

[23] A. Kamadan, G. Kiziltas, and V. Patoglu, "Co-design strategies for optimal variable stiffness actuation," *IEEE/ASME Transactions on Mechatronics*, vol. 22, no. 6, pp. 2768–2779, 2017.

[24] H. K. Fathy, P. Y. Papalambros, A. G. Ulsoy, and D. Hrovat, "Nested plant/controller optimization with application to combined passive/active automotive suspensions," in *Proceedings of the 2003 American Control Conference, 2003.*, vol. 4. IEEE, 2003, pp. 3375–3380.

[25] A. P. Deshmukh, D. R. Herber, and J. T. Allison, "Bridging the gap between open-loop and closed-loop control in co-design: A framework for complete optimal plant and control architecture design," in *2015 American Control Conference (ACC)*. IEEE, 2015, pp. 4916–4922.

[26] J. T. Allison, T. Guo, and Z. Han, "Co-design of an active suspension using simultaneous dynamic optimization," *Journal of Mechanical Design*, vol. 136, no. 8, 2014.

[27] O. L. De Weck, "Multiobjective optimization: History and promise," in *Invited Keynote Paper, GL2-2, The Third China-Japan-Korea Joint Symposium on Optimization of Structural and Mechanical Systems, Kanazawa, Japan*, vol. 2, 2004, p. 34.

[28] R. T. Marler and J. S. Arora, "Survey of multi-objective optimization methods for engineering," *Structural and multidisciplinary optimization*, vol. 26, no. 6, pp. 369–395, 2004.

[29] F. Helff, L. Gruenwald, and L. d'Orazio, "Weighted sum model for multi-objective query optimization for mobile-cloud database environments." in *EDBT/ICDT Workshops*, 2016.

[30] D. Isgro, G. Mantegazza, S. Formentin, G. Panzani, and S. M. Savaresi, "On-line data-based load classification in narrow-track vehicles," in *21st International Conference on Intelligent Transportation Systems*, 2018, pp. 3724–3729.

Giulio Panzani, M.Sc in Mechanical Engineering (2008) and Ph.D. in Information engineering (system control specialization, 2012) from Politecnico di Milano . He held post-doc positions at the University of Trento and at the Swiss Federal Institute of Technology of Zuerich (ETHZ). Since April 2015, he is assistant professor at Politecnico di Milano. His main research interests include the analysis of dynamics, control design and estimation for two (and four) wheeled vehicles and internal combustion engine control.

Davide Todeschini was born in Lecco (Italy) on January, 29th 1993. He received his Bachelor's Degree from Politecnico di Milano in 2015 and his Master's Degree cum Laude from Politecnico di Milano in 2017, discussing a thesis about the analysis and design of an electromechanical suspension for mountain bikes. From November 2017 he is PhD student at Politecnico di Milano, joining the mOve group.

Matteo Corno, M.Sc in computer and electrical engineering from the University of Illinois (2005), and Ph.D. from the Politecnico di Milano, Milano, Italy (2009). He is an Associate Professor with the Dipartimento di Elettronica, Informazione e Bioingegneria, Politecnico di Milano. He held research positions at U. of Minnesota, Johannes Kepler University, and TU Delft. His current research interests include dynamics and control of vehicles, Lithium-ion battery modelling, estimation and control.

Davide Sette is Control Systems and Innovation Supervisor at Ducati Motor Holding in Bologna, Italy. He graduated with a Master of Science degree in Electronic Engineering from Università di Padova and a specialization in Automatic Control Systems. He coordinates the design and development of electronic control systems and embedded software for two wheeled vehicles and the research on electronic innovation.

Sergio Savaresi, M.Sc. in Electrical Engineering (Politecnico di Milano, 1992), Ph.D. in Systems and Control Engineering (Politecnico di Milano, 1996), and M.Sc. in Applied Mathematics (Catholic University, Brescia, 2000). He is Full Professor in Automatic Control at Politecnico di Milano since 2006, and Chair of the Systems&Control Section of Department of Electronics and Computer Sciences, Politecnico di Milano. His main interests are in the areas of vehicles control, automotive systems, data analysis and system identification, non-linear control theory, and control applications.